Weak effects of electron-phonon interactions on the lattice thermal conductivity of wurtzite GaN with high electron concentrations

Jianshi Sun,[1] Shouhang Li,[1,*] Zhen Tong,[2] Cheng Shao,[3] Xiangchuan Chen,[1] Qianqian Liu,[1] Yucheng Xiong,[1] Meng An,[4] and Xiangjun Liu[1,†]

[1]*Institute of Micro/Nano Electromechanical System and Integrated Circuit, College of Mechanical Engineering, Donghua University, Shanghai 201620, China*

[2]*School of Advanced Energy, Sun Yat-Sen University, Shenzhen 518107, China*

[3]*Thermal Science Research Center, Shandong Institute of Advanced Technology, Jinan, Shandong 250103, China*

[4]*Department of Mechanical Engineering, University of Tokyo, 7-3-1 Hongo, Bunkyo, Tokyo 113-8656, Japan*

(Received 18 January 2024; accepted 25 March 2024; published 24 April 2024)

Wurtzite gallium nitride (GaN) has great potential for high-frequency and high-power applications due to its excellent electrical and thermal transport properties. However, enhancing the performance of GaN-based power electronics relies on heavy doping. Previous studies showed that electron-phonon interactions have strong effects on the lattice thermal conductivity of GaN due to the Fröhlich interaction. Surprisingly, our investigation reveals weak effects of electron-phonon interactions on the lattice thermal conductivity of *n*-type GaN at ultrahigh electron concentrations and the impact of the Fröhlich interaction can be ignored. The small phonon-electron scattering rate is attributed to the limited scattering channels, quantified by the Fermi surface nesting function. In contrast, there is a significant reduction in the lattice thermal conductivity of *p*-type GaN at high hole concentrations due to the relatively larger Fermi surface nesting function. Meanwhile, as *p*-type GaN has relatively smaller electron-phonon matrix elements, the reduction in lattice thermal conductivity is still weaker than that observed in *p*-type silicon. Our work provides a deep understanding of thermal transport in doped GaN and the conclusions can be further extended to other wide-band-gap semiconductors, including $\beta - Ga_2O_3$, AlN, and ZnO.

DOI: 10.1103/PhysRevB.109.134308

I. INTRODUCTION

GaN has a high Baliga figure of merit and large lattice thermal conductivity, which makes it promising for power electronics [1] and optoelectronics [2]. Generally, high charge carrier concentrations are required to obtain large electrical conductivity in GaN. For instance, when the hole concentration is increased to 2×10^{18} cm^{-3} doping with magnesium and oxygen atoms, the resistivity is reduced to 0.2 Ω cm [3]. Similarly, for *n*-type GaN, a high electrical conductivity exceeding 4×10^3 Ω^{-1} cm^{-1} is achieved with an electron concentration of 3.7×10^{20} cm^{-3} through germanium doping [4]. However, high-concentration doping can have a negative influence on the lattice thermal transport. An extra phonon scattering term, namely phonon-electron scattering, is introduced when there are plenty of charge carriers. This may lead to a pronounced reduction in lattice thermal conductivity, which is harmful to the performance of power semiconductor devices [5].

Thanks to the giant advancement in computational capability, it is possible to rigorously consider the electron-phonon interactions on the lattice thermal conductivity from first-principles calculations [6–8]. Liao *et al.* found that there is a significant reduction of ∼37% in lattice thermal conductivity for *n*-type silicon (Si) with an electron concentration of 10^{21} cm^{-3} [9]. Their predictions were later verified by the three-pulse femtosecond photoacoustic technique [10]. Similar trends were also observed in two-dimensional semiconductor materials, such as MoS_2 and PtSSe [11] and phosphorene and silicene [12]. Notably, GaN holds a much larger lattice thermal conductivity than Si because there is a large acoustic-optical phonon frequency gap which greatly limits available phonon-phonon scattering channels [13]. Given the weak phonon-phonon scattering, the phonon-electron scattering is expected to play a crucial role in GaN at high carrier concentrations, as observed in another wide-band-gap semiconductor 3C-SiC [14]. Previous studies by Yang *et al.* and Tang *et al.* reported that the lattice thermal conductivity of GaN is severely limited by the strong Fröhlich interaction between electrons and long-wavelength longitudinal optical phonons [15,16]. However, recent experiments showed that the thermal conductivity of *n*-type GaN is almost a constant within the concentration range of 10^{17} to 10^{19} cm^{-3} [17,18]. On the theoretical side, the lattice thermal conductivity of GaN matches experimental results better when accounting for four-phonon scattering [19]. It should be noted that electron-phonon interactions are not included in Ref. [19]. Therefore, the effect of electron-phonon interactions on the lattice thermal conductivity of GaN is still under debate.

*shouhang.li@dhu.edu.cn
†xjliu@dhu.edu.cn

In this work, the lattice thermal conductivities of *n*-type and *p*-type wurtzite GaN (space group $P6_3mc$, No. 186) under different carrier concentrations are investigated through mode-level first-principles calculations. It is found that the electron-phonon interactions have weak effects on the lattice thermal conductivity of *n*-type GaN even at an ultrahigh electron concentration. The impact of the Fröhlich interaction on lattice thermal conductivity can be ignored, which contradicts the previous understanding on the thermal transport in doped GaN, whereas there is a significant reduction in the lattice thermal conductivity of *p*-type GaN at high hole concentrations. We provide a comprehensive analysis of the contribution terms ascribed to electron-phonon interactions, including the electron density of states (DOS), Fermi surface nesting function, and electron-phonon matrix elements.

II. THEORY AND METHODS

Combining the linearized phonon BTE and Fourier's law, the lattice thermal conductivity (κ_{lat}) can be expressed as [20]

$$\kappa_{\text{lat},\alpha\beta} = \sum_{\lambda} c_{v,\lambda} v_{\lambda,\alpha} v_{\lambda,\beta} \tau_{\lambda} = \frac{1}{\Omega} \sum_{\lambda} \hbar\omega_{\lambda} \frac{\partial n_{\lambda}}{\partial T} v_{\lambda,\alpha} v_{\lambda,\beta} \tau_{\lambda}, \tag{1}$$

where α and β are the Cartesian coordinates, $\lambda \equiv (\mathbf{q}, \nu)$ denotes the phonon mode with wave vector $\mathbf{q}$ and phonon polarization ν, $c_{v,\lambda}$ is the phonon specific heat capacity, v_{λ} is the phonon group velocity, and τ_{λ} is the phonon relaxation time. Ω is the volume of the primitive cell, $\hbar$ is the reduced Planck's constant, ω_{λ} is the phonon frequency, and n_{λ} is the Bose-Einstein distribution at temperature T.

The essential step is to obtain τ_{λ}, which is associated with several scattering processes. The effective phonon scattering rates can be obtained using Matthiessen's rule: $1/\tau_{\lambda} = 1/\tau_{\lambda}^{\text{ph-ph}} + 1/\tau_{\lambda}^{\text{ph-iso}} + 1/\tau_{\lambda}^{\text{ph-el}}$, where $1/\tau_{\lambda}^{\text{ph-ph}}$ is the phonon-phonon scattering rates, $1/\tau_{\lambda}^{\text{ph-iso}}$ is the phonon-isotope scattering rates, and $1/\tau_{\lambda}^{\text{ph-el}}$ is the phonon-electron scattering rates.

According to Fermi's golden rule, the phonon-phonon scattering rates can be expressed as [21]

$$\frac{1}{\tau_{\lambda}^{\text{ph-ph}}} = 2\pi \sum_{\lambda_1\lambda_2} |V_{\lambda\lambda_1\lambda_2}|^2 \times \left[\frac{1}{2}\left(1 + n^0_{\lambda_1} + n^0_{\lambda_2}\right)\delta(\omega_{\lambda} - \omega_{\lambda_1} - \omega_{\lambda_2}) + \left(n^0_{\lambda_1} - n^0_{\lambda_2}\right)\delta(\omega_{\lambda} + \omega_{\lambda_1} - \omega_{\lambda_2})\right], \tag{2}$$

where $V_{\lambda\lambda_1\lambda_2}$ denote the three-phonon scattering matrix element. δ is the Dirac delta function which ensures the conservation of energy during the scattering processes. Recent studies have demonstrated that the four-phonon scattering has strong effects on lattice thermal conductivity at room temperature [22–26]. To evaluate the four-phonon scattering effects on κ_{lat} of GaN, we calculated the weighted phase space of three-phonon and four-phonon scattering. As shown in Fig. S1 of the Supplemental Material [27] (see also Refs. [28–33] therein), the weighted phase space of four-phonon scattering is significantly smaller than that for three-phonon scattering. Therefore, the four-phonon scattering has negligible effects on the lattice thermal conductivity of GaN at room temperature. The phonon-isotope scattering rates are evaluated by the Tamura theory and the details can be found in Ref. [34]. The phonon-electron scattering rates are related to the imaginary part of the phonon self-energy, which can be expressed as [35]

$$\frac{1}{\tau_{\lambda}^{\text{ph-el}}} = -\frac{2\pi}{\hbar} \sum_{mn,\mathbf{k}} \left|g^{v}_{mn}(\mathbf{k}, \mathbf{q})\right|^2 (f_{n\mathbf{k}} - f_{m\mathbf{k}+\mathbf{q}}) \times \delta(\varepsilon_{m\mathbf{k}+\mathbf{q}} - \varepsilon_{n\mathbf{q}} - \hbar\omega_{\lambda}), \tag{3}$$

where $g_{mn,v}(\mathbf{k}, \mathbf{q})$ is the electron-phonon matrix element, which quantifies probability amplitude for scattering between the electronic state $n\mathbf{k}$ and $m\mathbf{k} + \mathbf{q}$, f is the Fermi-Dirac distribution function, ε is the electron energy, and ε_F is the Fermi energy

The first-principles calculations are performed using the QUANTUM ESPRESSO package [36]. The electron exchange-correlation functional is treated by the generalized gradient approximation of Perdew, Burke, and Ernzerhof (PBE) [37] and optimized fully relativistic norm-conserving pseudopotentials [38] from PSEUDODOJO [39]. The kinetic energy cutoff for plane waves is set to be 100 Ry, and the convergence of electron energy is 10^{-10} Ry. It was shown that the spin-orbit coupling (SOC) has significant effects on the valance band structure in Ref. [40]. Therefore, the SOC is also included in our electronic band structure calculations. The harmonic and cubic force constants are calculated from density-functional perturbation theory. The electron-phonon interactions are first calculated under coarse $\mathbf{k}/\mathbf{q}$ meshes and then interpolated to dense meshes with the Wannier interpolation technique [41]. The convergence of phonon-electron scattering rates with respect to the $\mathbf{k}$-point mesh is verified in Fig. S2 of the Supplemental Material [27]. The in-house modified D3Q package [42] is employed to calculate the κ_{lat}, incorporating the phonon-electron scattering using the iterative calculation scheme [43–45]. The rigid shift of the Fermi energy is utilized to imitate the change of carrier concentration [46]. More details about the first-principles calculations are provided in the Supplemental Material [27].

III. RESULTS AND DISCUSSION

Figure 1(a) shows the electron band structure of GaN that includes the SOC effect. The Fermi energy corresponding to different carrier concentrations is represented by horizontal dashed lines. There is only one conduction band in the vicinity of the conduction band minimum (CBM), while there are multiple valance bands near the valence band maximum (VBM). Note that the heavy-hole and light-hole bands are split along the Γ-M high-symmetry path of the first Brillouin zone due to the SOC effects, as shown in Fig. S3(b) of the Supplemental Material [27]. This subtle variation, compared to the electronic band structure without SOC, has non-negligible effects on the electron-phonon interactions and the value of in-plane lattice thermal conductivity ($\kappa_{\text{lat},a}$) of *p*-type GaN, as shown in Table I. Our calculation shows that GaN is an indirect semiconductor with a band gap of 1.86 eV, strongly underestimating the measured value of 3.5 eV [47,48]. This is attributed to the well-known drawback in DFT [49].

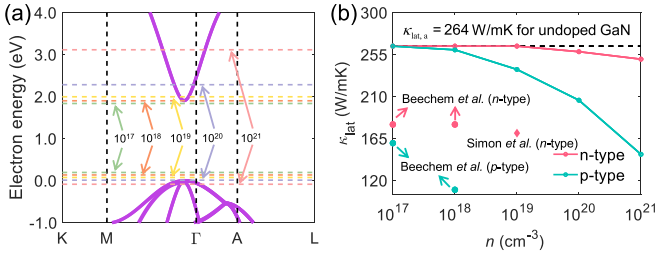

FIG. 1. (a) Band structures of GaN along the high-symmetry paths. The horizontal lines are Fermi energy related to the carrier concentrations of 10^{17} (green), 10^{18} (orange), 10^{19} (yellow), 10^{20} (light purple), and 10^{21} (light pink) cm^{-3} at room temperature. The electron energy is normalized to the VBM. (b) $\kappa_{1at,a}$ as a function of carrier concentration at room temperature for undoped, *n*-type, and *p*-type GaN. The scatters are experimental results, reported by Beechem *et al.* [17] and Simon *et al.* [18], respectively.

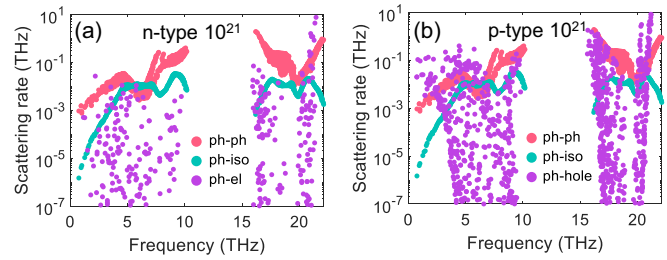

FIG. 2. $1/\tau_\lambda^{ph-ph}$, $1/\tau_\lambda^{ph-iso}$, (a) $1/\tau_\lambda^{ph-el}$, and (b) $1/\tau_\lambda^{ph-hole}$ at room temperature with carrier concentration of 10^{21} cm^{-3}.

However, this discrepancy has no influence on our conclusions on κ_{lat} since the profile of our DFT band structure matches well with the experimental results [50] and only the electron modes in the vicinity of the band edges have contributions to electron-phonon interactions. As for the phonon dispersion, our theoretical results agree well with the experimental data (Fig. S4 of the Supplemental Material [27]), which further confirms the reliability of our first-principles calculations.

The $\kappa_{1at,a}$ as a function of carrier concentrations (10^{17}–10^{21} cm^{-3}) for undoped, *n*-type, and *p*-type GaN are shown in Fig. 1(b). The $\kappa_{1at,a}$ at room temperature for undoped GaN, namely without phonon-electron scattering, is 264 W/mK, which is in good agreement with experimental [51,52] and former theoretical results [13]. With phonon-electron scattering included, the $\kappa_{1at,a}$ falls within the range of 250–258 W/mK for *n*-type GaN, which is quite close to the value of the undoped case. On the contrary, $\kappa_{1at,a}$ is dramatically reduced to 228 W/mK and 148 W/mK at the hole concentrations of 10^{19} cm^{-3} and 10^{21} cm^{-3}, respectively. A similar variation trend is also observed in time-domain thermoreflectance (TDTR) measurement [17,18], where the κ_{lat} of *n*-type GaN is almost a constant within the doping concentration range of 10^{17} to 10^{19} cm^{-3}. However, the κ_{lat} of *p*-type GaN exhibits a noticeable decrease. The quantitative differences between our work and Refs. [17,18] may be attributed to experimental sample sizes, impurities, or defects, which are not considered in our calculations. Recently, Pang *et al.* found that phonon-defect scattering can also have significant effects on the lattice thermal conductivity of 3C-SiC with B doping [53]. Here we mainly focus on the impact of electron-phonon interactions on lattice thermal conductivity. The phonon-defect scattering effects on the lattice thermal conductivity of GaN are out of the perspective of the present work and will be further discussed in future work.

TABLE I. $\kappa_{1at,a}$ of *n*-type and *p*-type GaN with and without SOC/polar effects. The carrier concentrations are 10^{21} cm^{-3} in all the cases.

$\kappa_{1at,a}$ (300 K)	With SOC	Without SOC	With Polar	Without Polar
n-type	250.34	249.59	250.34	246.51
p-type	147.85	125.51	147.85	146.20

The effects of electron-phonon interactions on κ_{lat} are significantly different from the observations in Si [9] and 3C-SiC [14]. Both electron and hole have strong interactions with phonons, resulting in a substantial decrease in κ_{lat} [9]. Since the $1/\tau_\lambda^{ph-ph}$ for phonon frequencies of GaN below 10 THz is smaller than that in Si (Fig. S5 of the Supplemental Material [27]), the nearly flat κ_{lat} with different concentrations of *n*-type GaN is anomalous. To reveal the underlying mechanisms, the mode-level phonon-electron and phonon-hole scattering rates at the carrier concentration of 10^{21} cm^{-3} are calculated, as shown in Figs. 2(a) and 2(b), respectively. The scattering rates at other carrier concentrations are also provided in Fig. S6 of the Supplemental Material [27]. Remarkably, $1/\tau_\lambda^{ph-el}$ is significantly lower than $1/\tau_\lambda^{ph-ph}$ for low-frequency phonons (below 10 THz), which have the main contribution to κ_{lat} [54,55]. In contrast, $1/\tau_\lambda^{ph-hole}$ is significantly larger than $1/\tau_\lambda^{ph-ph}$ within the same frequency range. Note that $1/\tau_\lambda^{ph-el}$ and $1/\tau_\lambda^{ph-hole}$ for high-frequency optical phonons (above 15 THz) become even larger due to the Fröhlich interaction in polar materials [56]. This phenomenon is also observed in Ref. [15]. However, optical phonon modes have an ignorable contribution to the κ_{lat} of GaN [54]. Therefore, the strong Fröhlich interaction does not lead to a large reduction in κ_{lat} of GaN. This hypothesis is further verified by the calculated $\kappa_{1at,a}$ with/without considering the Fröhlich interaction, as shown in Table I.

The distinctions in $1/\tau_\lambda^{ph-el}$ and $1/\tau_\lambda^{ph-hole}$ at the same concentration are primarily attributed to the distinctions in electron DOS within the Fermi window regarding *n*-type and *p*-type GaN. GaN becomes a degenerate semiconductor when the carrier concentration reaches 10^{21} cm^{-3} for both *n*-type and *p*-type. Therefore, the Fermi energy moves into the conduction band or the valence band. As shown in Fig. 3(a), the DOS for holes is notably larger than that for electrons at 10^{21} cm^{-3}. It should be noted that the DOS exhibits a pronounced asymmetric profile. As shown in Fig. S7 of the Supplemental Material [27], the DOS in the vicinity of the VBM is primarily contributed by *p* orbitals, which exhibit a triple degeneracy and minimal band dispersion. Conversely, the vicinity of the CBM is primarily contributed by *s* orbitals, resulting in nondegenerate and dispersive electron bands [57–59]. According to Eq. (3) and its variant based on the double-delta approximation [44,60,61], the DOS determines the Fermi surface nesting function ($\zeta_\mathbf{q}$) to a large extent, which

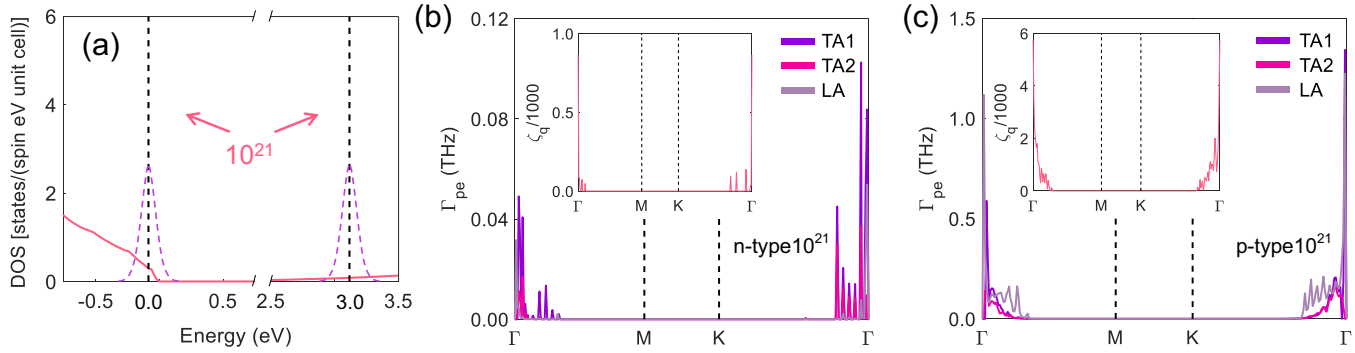

FIG. 3. (a) Electron DOS near the valence- and conduction-band edges. The purple dotted curve represents the Fermi window. The electron energy is normalized to the VBM. The position of the Fermi energy for electron and hole concentrations of 10^{21} cm^{-3} is indicated with black dashed lines. Room-temperature phonon linewidth Γ_{pe} of TA1, TA2, and LA along the high-symmetry path due to (b) phonon-electron and (c) phonon-hole scattering with carrier concentration of 10^{21} cm^{-3}. The Fermi surface nesting function is inserted to the top left in (b) and (c).

is expressed as

$$\zeta_{\mathbf{q}} = \sum \delta(\varepsilon_{n\mathbf{k}} - \varepsilon_F)\delta(\varepsilon_{m\mathbf{k}+\mathbf{q}} - \varepsilon_F). \tag{4}$$

$\zeta_{\mathbf{q}}$ quantifies the phonon-electron scattering channels [62]. The phonon linewidth with respect to the phonon-electron scattering ($\Gamma_{pe} = 1/2\tau_\lambda^{ph-el}$) and $\zeta_{\mathbf{q}}$ of the two transverse acoustic phonon branches (TA1 and TA2), as well as the longitudinal acoustic phonon branch (LA), are shown in Figs. 3(b) and 3(c). The $\zeta_{\mathbf{q}}$ in the vicinity of the Γ point is quite large due to the collinearity of electron group velocities $\mathbf{v}_{\mathbf{k}}$ and $\mathbf{v}_{\mathbf{k}} + \mathbf{q}$ [63]. The $\zeta_{\mathbf{q}}$ of *n*-type GaN is much lower than that of *p*-type GaN, which results in its relatively smaller Γ_{pe}. Therefore, the electron-phonon interactions have weak effects on the κ_{lat} of *n*-type GaN, while they have strong effects on that of *p*-type GaN. This conclusion can be further extended to other wide-band-gap semiconductors, like $\beta - Ga_2O_3$, AlN, and ZnO [64], whose electron DOS is relatively larger than the hole DOS.

We further compare the κ_{lat} of Si and GaN for both *n*-type and *p*-type at the carrier concentration of 10^{21} cm^{-3}. The κ_{lat} of *n*-type Si is reduced by ∼37% [9] due to phonon-electron scattering, while the *n*-type GaN is reduced only by 2.85% in our calculation. As shown in Fig. 4(a), $1/\tau_\lambda^{ph-el}$ is larger than $1/\tau_\lambda^{ph-ph}$ for plenty of low-frequency phonons in Si. As a contrast, fewer phonon modes have larger $1/\tau_\lambda^{ph-el}$ than $1/\tau_\lambda^{ph-ph}$ in GaN. This discrepancy can be attributed to differences in electron DOS. As shown in Fig. 4(b), the electron DOS of Si is much larger than that of GaN at the electron concentration of 10^{21} cm^{-3}. Note that the hole DOS of GaN is close to that of Si at the hole concentration of 10^{21} cm^{-3}. Nevertheless, the κ_{lat} of Si is decreased by 45%, while that of GaN is decreased by a smaller value of 29%. As shown in Fig. S8 of the Supplemental Material [27], the $\zeta_{\mathbf{q}}$ of *p*-type GaN is much larger than that of *p*-type Si, which cannot interpret the discrepancy in their κ_{lat}. According to Eq. (3), the $1/\tau_\lambda^{ph-el}$ is also related to electron-phonon matrix elements *g*, which quantifies the coupling strength between phonon modes and electron states,

$$g_{mn}^{v}(\mathbf{k}, \mathbf{q}) = \sqrt{\frac{\hbar}{2\omega_\lambda}} \langle \psi_{m\mathbf{k}+\mathbf{q}} | \partial_\lambda V | \psi_{n\mathbf{k}} \rangle, \tag{5}$$

with ψ the ground-state Bloch wave function and $\partial_\lambda V$ the first-order derivative of the Kohn-Sham potential with respect to the atomic displacement. As shown in Fig. 4(c), the magnitude of $|g|$ for Si is larger than that for GaN, resulting in the smaller κ_{lat} for Si. Recent studies have demonstrated that

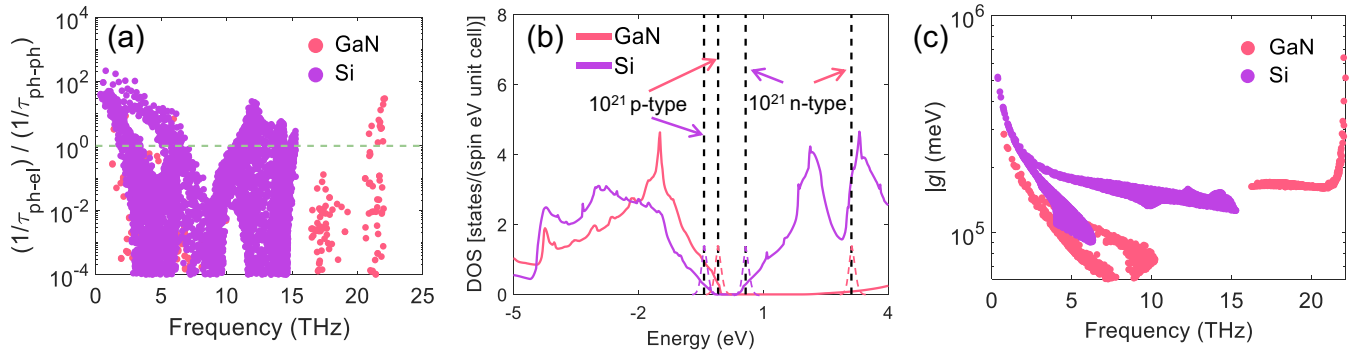

FIG. 4. (a) The ratio of $1/\tau_\lambda^{ph-el}$ to $1/\tau_\lambda^{ph-ph}$ with 10^{21} cm^{-3} electron concentration of GaN and Si, which is used to identify the dominant scattering term in phonon thermal transport. The horizon green line marks the equal importance of $1/\tau_\lambda^{ph-el}$ and $1/\tau_\lambda^{ph-ph}$. (b) The DOS for GaN and Si. The positions of the Fermi energy for the electron and hole concentrations of 10^{21} cm^{-3} are indicated with black dashed lines for GaN and Si. The purple and red dotted curves represent Fermi windows. (c) Absolute value of electron-phonon matrix elements $|g|$ of GaN and Si.

a 2% biaxial tensile strain can increase the hole mobility of GaN by 230% [40,65], which indicates great promise for the application of *p*-type GaN in power electronics. However, our findings reveal that electron-phonon interactions can significantly limit κ_{lat} of *p*-type GaN. Therefore, it is not only urgent to synthesize high-quality *p*-type GaN samples but also important to overcome the challenges in the thermal management of power electronics based on *p*-type GaN in the future.

IV. CONCLUSIONS

In summary, the lattice thermal conductivities of *n*-type and *p*-type GaN are investigated through mode-level first-principles calculations. The effects of electron-phonon interactions on the lattice thermal conductivity are shown to be weak in *n*-type GaN, even at an ultrahigh electron concentration of 10^{21} cm^{-3}. Intriguingly, our findings indicate that the Fröhlich interaction has an ignorable influence on the lattice thermal conductivity. The weak phonon-electron scattering is attributed to the limited scattering channels, which is reflected by the Fermi surface nesting function. In addition, our study reveals that the electron-phonon interactions significantly limit the lattice thermal conductivities of *p*-type GaN and Si. Importantly, it is the electron-phonon matrix elements, rather than the Fermi surface nesting function, that are ascribed to the relatively larger reduction in the thermal conductivity of *p*-type Si compared to *p*-type GaN.

ACKNOWLEDGMENTS

S.L. was supported by the National Natural Science Foundation of China (Grant No. 12304039), the Shanghai Municipal Natural Science Foundation (Grant No. 22YF1400100), the Fundamental Research Funds for the Central Universities (Grant No. 2232022D-22), and the startup funding for youth faculty from the College of Mechanical Engineering of Donghua University. X.L. was supported by the Shanghai Municipal Natural Science Foundation (Grant No. 21TS1401500) and the National Natural Science Foundation of China (Grants No. 52150610495 and No. 12374027).

[1] F. Roccaforte, P. Fiorenza, G. Greco, R. L. Nigro, F. Giannazzo, F. Iucolano, and M. Saggio, Emerging trends in wide band gap semiconductors (SiC and GaN) technology for power devices, Microelectron. Eng. **187-188**, 66 (2018).

[2] K. Chung, C.-H. Lee, and G.-C. Yi, Transferable GaN layers grown on ZnO-coated graphene layers for optoelectronic devices, Science **330**, 655 (2010).

[3] R. Korotkov, J. Gregie, and B. W. Wessels, Electrical properties of *p*-type GaN: Mg codoped with oxygen, Appl. Phys. Lett. **78**, 222 (2001).

[4] L. Konczewicz, E. Litwin-Staszewska, M. Zajac, H. Turski, M. Bockowski, D. Schiavon, M. Chlipała, M. Iwinska, P. Nita, S. Juillaguet *et al.*, Electrical transport properties of highly doped n-type GaN materials, Semicond. Sci. Technol. **37**, 055012 (2022).

[5] R. J. Warzoha, A. A. Wilson, B. F. Donovan, N. Donmezer, A. Giri, P. E. Hopkins, S. Choi, D. Pahinkar, J. Shi, S. Graham *et al.*, Applications and impacts of nanoscale thermal transport in electronics packaging, J. Electron. Packag. **143**, 020804 (2021).

[6] Z. Tong, S. Li, X. Ruan, and H. Bao, Comprehensive first-principles analysis of phonon thermal conductivity and electron-phonon coupling in different metals, Phys. Rev. B **100**, 144306 (2019).

[7] A. Jain and A. J. McGaughey, Thermal transport by phonons and electrons in aluminum, silver, and gold from first principles, Phys. Rev. B **93**, 081206(R) (2016).

[8] Y. Chen, J. Ma, and W. Li, Understanding the thermal conductivity and Lorenz number in tungsten from first principles, Phys. Rev. B **99**, 020305(R) (2019).

[9] B. Liao, B. Qiu, J. Zhou, S. Huberman, K. Esfarjani, and G. Chen, Significant reduction of lattice thermal conductivity by the electron-phonon interaction in silicon with high carrier concentrations: A first-principles study, Phys. Rev. Lett. **114**, 115901 (2015).

[10] B. Liao, A. Maznev, K. A. Nelson, and G. Chen, Photo-excited charge carriers suppress sub-terahertz phonon mode in silicon at room temperature, Nat. Commun. **7**, 13174 (2016).

[11] C. Liu, M. Yao, J. Yang, J. Xi, and X. Ke, Strong electron-phonon interaction induced significant reduction in lattice thermal conductivities for single-layer MoS_2 and PtSSe, Mater. Today Phys. **15**, 100277 (2020).

[12] S.-Y. Yue, R. Yang, and B. Liao, Controlling thermal conductivity of two-dimensional materials via externally induced phonon-electron interaction, Phys. Rev. B **100**, 115408 (2019).

[13] L. Lindsay, D. A. Broido, and T. L. Reinecke, Thermal conductivity and large isotope effect in GaN from first principles, Phys. Rev. Lett. **109**, 095901 (2012).

[14] T. Wang, Z. Gui, A. Janotti, C. Ni, and P. Karandikar, Strong effect of electron-phonon interaction on the lattice thermal conductivity in 3C-SiC, Phys. Rev. Mater. **1**, 034601 (2017).

[15] J.-Y. Yang, G. Qin, and M. Hu, Nontrivial contribution of Fröhlich electron-phonon interaction to lattice thermal conductivity of wurtzite GaN, Appl. Phys. Lett. **109**, 242103 (2016).

[16] D.-S. Tang, G.-Z. Qin, M. Hu, and B.-Y. Cao, Thermal transport properties of GaN with biaxial strain and electron-phonon coupling, J. Appl. Phys. **127**, 035102 (2020).

[17] T. E. Beechem, A. E. McDonald, E. J. Fuller, A. A. Talin, C. M. Rost, J.-P. Maria, J. T. Gaskins, P. E. Hopkins, and A. A. Allerman, Size dictated thermal conductivity of GaN, J. Appl. Phys. **120**, 095104 (2016).

[18] R. B. Simon, J. Anaya, and M. Kuball, Thermal conductivity of bulk GaN—Effects of oxygen, magnesium doping, and strain field compensation, Appl. Phys. Lett. **105**, 202105 (2014).

[19] X. Yang, T. Feng, J. Li, and X. Ruan, Stronger role of four-phonon scattering than three-phonon scattering in thermal conductivity of III-V semiconductors at room temperature, Phys. Rev. B **100**, 245203 (2019).

[20] D. A. Broido, M. Malorny, G. Birner, N. Mingo, and D. Stewart, Intrinsic lattice thermal conductivity of semiconductors from first principles, Appl. Phys. Lett. **91**, 231922 (2007).

[21] R. Albers, L. Bohlin, M. Roy, and J. Wilkins, Normal and umklapp phonon decay rates due to phonon-phonon and electron-phonon scattering in potassium at low temperatures, Phys. Rev. B **13**, 768 (1976).

[22] Y. Zhao, S. Zeng, G. Li, C. Lian, Z. Dai, S. Meng, and J. Ni, Lattice thermal conductivity including phonon frequency shifts and scattering rates induced by quartic anharmonicity in cubic oxide and fluoride perovskites, Phys. Rev. B **104**, 224304 (2021).

[23] Y. Zhao, C. Lian, S. Zeng, Z. Dai, S. Meng, and J. Ni, Anomalous electronic and thermoelectric transport properties in cubic Rb_3 AuO antiperovskite, Phys. Rev. B **102**, 094314 (2020).

[24] Y. Zhao, C. Lian, S. Zeng, Z. Dai, S. Meng, and J. Ni, Quartic anharmonicity and anomalous thermal conductivity in cubic antiperovskites A_3BO (A = K, Rb; B = Br, Au), Phys. Rev. B **101**, 184303 (2020).

[25] T. Yue, Y. Zhao, J. Ni, S. Meng, and Z. Dai, Microscopic mechanism of low lattice thermal conductivity in natural superlattice materials BaXYF (X = Cu, Ag; Y = Se, Te) including fully quartic anharmonicity, Phys. Rev. B **107**, 024301 (2023).

[26] T. Feng, L. Lindsay, and X. Ruan, Four-phonon scattering significantly reduces intrinsic thermal conductivity of solids, Phys. Rev. B **96**, 161201(R) (2017).

[27] See Supplemental Material at http://link.aps.org/supplemental/10.1103/PhysRevB.109.134308 for detailed information regarding computational details, weighted phase space for three-phonon and four-phonon scattering, convergence tests on **k**-point mesh, band structure with and without spin-orbit coupling, phonon dispersion, phonon-phonon scattering rates, phonon-electron scattering rates, total and partial electron density of states, and Fermi surface nesting function.

[28] C. G. Broyden, The convergence of a class of double-rank minimization algorithms 1. General considerations, J. Inst. Math. Its Appl. **6**, 76 (1970).

[29] D. Goldfarb, A family of variable-metric methods derived by variational means, Math. Comput. **24**, 23 (1970).

[30] D. F. Shanno, Conditioning of quasi-Newton methods for function minimization, Math. Comput. **24**, 647 (1970).

[31] M. Straumanis and E. Aka, Lattice parameters, coefficients of thermal expansion, and atomic weights of purest silicon and germanium, J. Appl. Phys. **23**, 330 (1952).

[32] H. Schulz and K. H. Thiemann, Crystal structure refinement of AlN and GaN, Solid State Commun. **23**, 815 (1977).

[33] T. Ruf, J. Serrano, M. Cardona, P. Pavone, M. Pabst, M. Krisch, M. D'Astuto, T. Suski, I. Grzegory, and M. Leszczynski, Phonon dispersion curves in wurtzite-structure GaN determined by inelastic x-ray scattering, Phys. Rev. Lett. **86**, 906 (2001).

[34] S.-i. Tamura, Isotope scattering of dispersive phonons in Ge, Phys. Rev. B **27**, 858 (1983).

[35] S. Poncé, E. R. Margine, C. Verdi, and F. Giustino, EPW: Electron-phonon coupling, transport and superconducting properties using maximally localized Wannier functions, Comput. Phys. Commun. **209**, 116 (2016).

[36] P. Giannozzi, S. Baroni, N. Bonini, M. Calandra, R. Car, C. Cavazzoni, D. Ceresoli, G. L. Chiarotti, M. Cococcioni, I. Dabo *et al.*, QUANTUM ESPRESSO: A modular and open-source software project for quantum simulations of materials, J. Phys.: Condens. Matter **21**, 395502 (2009).

[37] J. P. Perdew, A. Ruzsinszky, G. I. Csonka, O. A. Vydrov, G. E. Scuseria, L. A. Constantin, X. Zhou, and K. Burke, Restoring the density-gradient expansion for exchange in solids and surfaces, Phys. Rev. Lett. **100**, 136406 (2008).

[38] D. R. Hamann, Optimized norm-conserving Vanderbilt pseudopotentials, Phys. Rev. B **88**, 085117 (2013).

[39] M. J. van Setten, M. Giantomassi, E. Bousquet, M. J. Verstraete, D. R. Hamann, X. Gonze, and G.-M. Rignanese, The PSEUDODOJO: Training and grading a 85 element optimized norm-conserving pseudopotential table, Comput. Phys. Commun. **226**, 39 (2018).

[40] S. Poncé, D. Jena, and F. Giustino, Route to high hole mobility in GaN via reversal of crystal-field splitting, Phys. Rev. Lett. **123**, 096602 (2019).

[41] N. Marzari, A. A. Mostofi, J. R. Yates, I. Souza, and D. Vanderbilt, Maximally localized Wannier functions: Theory and applications, Rev. Mod. Phys. **84**, 1419 (2012).

[42] L. Paulatto, F. Mauri, and M. Lazzeri, Anharmonic properties from a generalized third-order *ab initio* approach: Theory and applications to graphite and graphene, Phys. Rev. B **87**, 214303 (2013).

[43] S. Li, Z. Tong, C. Shao, H. Bao, T. Frauenheim, and X. Liu, Anomalously isotropic electron transport and weak electron-phonon interactions in hexagonal noble metals, J. Phys. Chem. Lett. **13**, 4289 (2022).

[44] S. Li, A. Wang, Y. Hu, X. Gu, Z. Tong, and H. Bao, Anomalous thermal transport in metallic transition-metal nitrides originated from strong electron-phonon interactions, Mater. Today Phys. **15**, 100256 (2020).

[45] J. Sun, G. Chen, S. Li, and X. Liu, Light atomic mass induces low lattice thermal conductivity in Janus transition-metal dichalcogenides MSSe (M = Mo, W), J. Phys. Chem. C **127**, 17567 (2023).

[46] S. Li, Z. Tong, and H. Bao, Resolving different scattering effects on the thermal and electrical transport in doped SnSe, J. Appl. Phys. **126**, 025111 (2019).

[47] R. Dingle, D. Sell, S. Stokowski, and M. Ilegems, Absorption, reflectance, and luminescence of GaN epitaxial layers, Phys. Rev. B **4**, 1211 (1971).

[48] B. Monemar, Fundamental energy gap of GaN from photoluminescence excitation spectra, Phys. Rev. B **10**, 676 (1974).

[49] M. K. Y. Chan and G. Ceder, Efficient band gap prediction for solids, Phys. Rev. Lett. **105**, 196403 (2010).

[50] A. V. Rodina, M. Dietrich, A. Göldner, L. Eckey, A. Hoffmann, A. L. Efros, M. Rosen, and B. K. Meyer, Free excitons in wurtzite GaN, Phys. Rev. B **64**, 115204 (2001).

[51] A. Jeżowski, P. Stachowiak, T. Plackowski, T. Suski, S. Krukowski, M. Boćkowski, I. Grzegory, B. Danilchenko, and T. Paszkiewicz, Thermal conductivity of GaN crystals grown by high pressure method, Phys. Status Solidi B **240**, 447 (2003).

[52] G. A. Slack, L. J. Schowalter, D. Morelli, and J. A. Freitas Jr., Some effects of oxygen impurities on AlN and GaN, J. Cryst. Growth **246**, 287 (2002).

[53] G. Pang, F. Meng, Y. Chen, A. Katre, J. Carrete, B. Dongre, G. K. Madsen, N. Mingo, and W. Li, Thermal conductivity reduction in highly-doped cubic SiC by phonon-defect and phonon-electron scattering, Mater. Today Phys. **41**, 101346 (2024).

[54] X. Wu, J. Lee, V. Varshney, J. L. Wohlwend, A. K. Roy, and T. Luo, Thermal conductivity of wurtzite zinc-oxide from first-principles lattice dynamics—a comparative study with gallium nitride, Sci. Rep. **6**, 22504 (2016).

[55] J. Garg, T. Luo, and G. Chen, Spectral concentration of thermal conductivity in GaNA first-principles study, Appl. Phys. Lett. **112**, 252101 (2018).

[56] S. Sheih, K.-T. Tsen, D. Ferry, A. Botchkarev, B. Sverdlov, A. Salvador, and H. Morkoc, Electron-phonon interactions in the wide band-gap semiconductor GaN, Appl. Phys. Lett. **67**, 1757 (1995).

[57] K. Yoodee, J. C. Woolley, and V. Sa-Yakanit, Effects of *p-d* hybridization on the valence band of I-III-$\mathbf{VI}_2$ chalcopyrite semiconductors, Phys. Rev. B **30**, 5904 (1984).

[58] D. C. Reynolds, D. C. Look, B. Jogai, C. W. Litton, G. Cantwell, and W. C. Harsch, Valence-band ordering in ZnO, Phys. Rev. B **60**, 2340 (1999).

[59] A. Walsh, J. L. F. Da Silva, and S.-H. Wei, Origins of band-gap renormalization in degenerately doped semiconductors, Phys. Rev. B **78**, 075211 (2008).

[60] Y. Wang, Z. Lu, and X. Ruan, First principles calculation of lattice thermal conductivity of metals considering phonon-phonon and phonon-electron scattering, J. Appl. Phys. **119**, 225109 (2016).

[61] S. Li, X. Zhang, and H. Bao, Thermal transport by electrons and phonons in $PdTe_2$: An *ab initio* study, Phys. Chem. Chem. Phys. **23**, 5956 (2021).

[62] C. Li, N. K. Ravichandran, L. Lindsay, and D. Broido, Fermi surface nesting and phonon frequency gap drive anomalous thermal transport, Phys. Rev. Lett. **121**, 175901 (2018).

[63] D. Kasinathan, J. Kuneš, A. Lazicki, H. Rosner, C. S. Yoo, R. T. Scalettar, and W. E. Pickett, Superconductivity and lattice instability in compressed lithium from Fermi surface hot spots, Phys. Rev. Lett. **96**, 047004 (2006).

[64] S. Curtarolo, W. Setyawan, G. L. Hart, M. Jahnatek, R. V. Chepulskii, R. H. Taylor, S. Wang, J. Xue, K. Yang, O. Levy *et al.*, AFLOW: An automatic framework for high-throughput materials discovery, Comput. Mater. Sci. **58**, 218 (2012).

[65] S. Poncé, D. Jena, and F. Giustino, Hole mobility of strained GaN from first principles, Phys. Rev. B **100**, 085204 (2019).